Applied Mathematics and Computation 414 (2022) 126669

Contents lists available at ScienceDirect

Applied Mathematics and Computation

journal homepage: www.elsevier.com/locate/amc

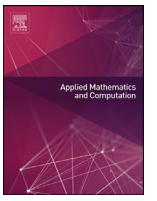

Highly efficient Shannon wavelet-based pricing of power options under the double exponential jump framework with stochastic jump intensity and volatility

Chun-Sung Huang[a,*], John G. O'Hara[b], Sure Mataramvura[c]

[a] Department of Finance & Tax, University of Cape Town, Rondebosch 7701, South Africa
[b] Department of Mathematical Sciences, University of Essex, Colchester CO4 3SQ, UK
[c] Division of Actuarial Sciences, University of Cape Town, Rondebosch 7701, South Africa

ARTICLE INFO

Article history:
Received 13 April 2019
Revised 24 August 2021
Accepted 15 September 2021
Available online 2 October 2021

Keywords:
Shannon wavelets
Fourier transform inversion
Power options
Double exponential jumps
Stochastic volatility
Stochastic jump intensity

ABSTRACT

We propose a highly efficient and accurate valuation method for exotic-style options based on the novel Shannon wavelet inverse Fourier technique (SWIFT). Specifically, we derive an efficient pricing method for power options under a more realistic double exponential jump model with stochastic volatility and jump intensity. The inclusion of such innovations may accommodate for the various stylised facts observed in the prices of financial assets, and admits a more realistic pricing framework as a result. Following the derivation of our SWIFT pricing method for power options, we perform extensive numerical experiments to analyse both the method's accuracy and efficiency. In addition, we investigate the sensitivities in the resulting prices, as well as the inherent errors, to changes in the underlying market conditions. Our numerical results demonstrate that the SWIFT method is not only more efficient when benchmarked to its closest competitors, such as the Fourier-cosine (COS) and the widely-acclaimed fast-Fourier transform (FFT) methods, but it is also robust across a range of different market conditions exhibiting exponential error convergence.

1. Introduction

A power (or leverage) option is an exotic derivative characterised by its payoff at maturity, whereby the underlying asset price is raised to some constant power. Such deviations from the typical plain vanilla option with a linear payoff allows for the hedging of non-linear risk [30]. Moreover, power options can also be used as an effective leveraging tool. The leverage can be magnified by allowing the power to be greater than 1, such that a small change in the underlying price will lead to a significant change in the price of the option [34]. This can provide bullish traders of call options more benefits than simply using a standard plain vanilla option.

Power options are commonly traded in the financial market. For example, capped power options on forex was issued by the Bankers Trust in Germany. Additionally, power options whereby the final payoff at maturity is a polynomial function of the Nikkei level was widely traded on the Tokyo Stock Exchange (see [10,23,30,31]). However, despite its popularity

* Corresponding author.
E-mail address: chun-sung.huang@uct.ac.za (C.-S. Huang).

https://doi.org/10.1016/j.amc.2021.126669

and the aforementioned advantages, there is limited research for pricing of power options (see [12,17,18] for some examples). In particular, to the best of our knowledge, there is a gap in the current literature on the efficient pricing of power options, especially under a more realistic double-exponential jump framework for the underlying price. Notably, with the advent of high frequency trading in the financial market, efficient pricing methods to obtain option values become ever more prominent for practitioners and academics alike. In addition, under a more sophisticated framework of asset price dynamics, efficient pricing techniques are also required in practice to quickly calibrate the model parameters to the existing market data, which usually involves repeated pricing of a basket of options across a wide range of strikes.

In this paper, we will explore the avenue of efficient pricing of power options under a framework whereby the underlying asset price is governed by a double-exponential jump model. Specifically, we allow both the underlying volatility and the intensity of jumps to be driven by separate stochastic processes. The proposed asset price model is motivated by a wealth of advantages. Firstly, embracing double-exponential jumps will allow us to capture events of extreme price movements, such as a financial crisis, as well as the asymmetry leptokurtic feature embedded in the distribution of financial asset returns [20,21]. Secondly, by incorporating stochastic volatility we may account for the volatility smile or smirk features commonly observed in the financial market [9,15]. Finally, allowing the jump intensity to follow its own mean-reverting stochastic process will accommodate for (i) switches in jump intensity over time [2], (ii) the lack of correlation between the jump intensity and the diffusive volatility [29], as well as (iii) the mean-reverting property embedded in the jumps [13].

In our proposed work, we investigate the highly efficient Shannon wavelet inverse Fourier technique (SWIFT) option pricing method, introduced through the seminal work of [25], and compare the resulting accuracy and computational efficiency to that of the widely-acclaimed fast Fourier transform (FFT) of [1] and its more recent alternative, the Fourier-cosine (COS) method of [5]. While the FFT is a well-established method among practitioners and academics alike, the latter has received recognition to be the more efficient alternative since its inception a decade ago. However, unlike the FFT, the COS method does not depend on the selection of an arbitrary damping factor for convergence, albeit having restrictions of its own. Drawbacks of the COS method include the choice of an appropriate integration bound in order to capture an adequate mass of the underlying density function, which is critical given the heavy-tailed nature of the density functions that are commonly observed in finance. However, there is no existing algorithm to select the most suitable integration range for all asset price processes, nor for the type of option to be priced.

Our inclusion of the COS method as an additional benchmark model to measure accuracy and efficiency is consistent with the seminal work of [25], as well as its extensions thereof (for instance, see [3,22,24]). While the choice of the half-range Fourier-cosine series (of the COS method) over the half-range Fourier-sine and the full-range Fourier-sine-cosine series is not immediately obvious, it is not without its merits. Notably, the fruitful work of [16] determined that the Fourier-sine series approximation is the least effective of these three Fourier series algorithms. In addition, the full-range Fourier-sine-cosine series only outperforms the COS method when pricing out-of-the-money call options with short maturities (three months or less), albeit at the cost of imposing a relatively large approximation interval to recover the density function (see [16]). It is also worthwhile emphasising that the COS method has attracted considerable attention and is more widely-researched in comparison to its closest competitors. Consequently, the COS method's robustness and effectiveness are also more evidently demonstrated through a wealth of existing literature (see, among others, [6,7,11,14,28,32,35,36]). Hence, the natural consideration of the COS method as a benchmark to measure our pricing efficacy may be deemed appropriate in this scope of work.

The SWIFT method belongs to a family of wavelet-based pricing techniques, which are generally more flexible and accurate for the valuation of options with longer time to expiry [24,25]. Indeed, the SWIFT method does not require prior decisions on the truncation of the integration range, and can accurately price both long- and short-dated options. This is one of the main improvements over the COS method. In addition, since Shannon wavelets are smooth, we can expect an accurate approximation of heavy-tailed density functions that often emerge in finance. The accuracy and error convergence of the SWIFT method, however, relies heavily on the selection of an appropriate scale of approximation. We shall explore three separate methods in our numerical examples to identify the most adequate choice of such a scale for the pricing of power options.

The reasons to explore the above-mentioned state-of-the-art numerical integration techniques is non-trivial, and we shall provide further justification in the sequel. Firstly, while the double-exponential jump framework may account for the various empirical features mentioned above, and allow pricing models to more accurately value financial derivatives as a result, it is worthwhile highlighting that, due to the additional level of complexity introduced under such a framework, a closed-form solution of the density function governing the underlying stochastic price process is not readily available. Hence, the classical option valuation through the discounted expectation of the final payoff under the risk-neutral measure breaks down. However, since the associated characteristic function, defined as the Fourier transform of the density function, is more easily obtainable, pricing of the power option in question can be explored with numerical integration techniques in the Fourier space instead. Secondly, prior literature has demonstrated extensive that pricing in the Fourier domain may be more computationally efficient (see, among others, [1,5,11–13,17,19,24–26]), which addresses our above-mentioned concern regarding the necessity of implementing more efficient pricing methods in practice. Finally, to the best of our knowledge, while both the SWIFT and the COS method has been shown by prior research to be robust under common Lévy type models, a gap exists in the current literature that explores the efficiency and robustness of these methods in a more realistic, albeit sophisticated, setting such as our proposed double-exponential jump framework. In addition, whether such valuation techniques remain

rigorous when pricing more exotic-style derivatives will require further investigation. Hence, our contribution in this paper also forms a natural extension to the seminal work of both [5] and [25].

Specifically, the aforementioned extension includes further investigation and demonstration of the SWIFT and COS methods' tractability in pricing derivatives beyond the vanilla-type, such as exploring the exotic-styled power options justified above. More importantly, our proposed work examines the SWIFT and COS methods' ability to value options accurately and efficiently under the more realistic double-exponential jump framework for the first time, while advocating for both the volatility and jump intensity processes to be stochastic in nature. The inclusion of such innovations will more accurately capture the various phenomena and stylised facts observed in the financial market, and will test the pricing methods' performance when valuing derivatives in a more realistic setting. To the best of the authors' knowledge, the proposed work investigates the SWIFT and COS methods' robustness, accuracy and efficiency under such a framework for the first time.

Our numerical experiments will focus on comparing the accuracy and efficiency of the SWIFT method to that of the novel COS method in a setting whereby randomness is introduced in both the underlying volatility and jump intensity, particularly for the pricing of power options. Further to the pricing, we investigate the sensitivity of the resulting power option prices to changes in the underlying parameters for model robustness. This work contributes to the body of knowledge in two main ways. Firstly, we provide strong evidence to demonstrate the superior efficiency of the proposed SWIFT method over the COS method, which has been shown in recent literature to be the preferred method over the widely-acclaimed FFT method. Secondly, we provide various numerical examples to analyse the resulting errors and price sensitivities to demonstrate the SWIFT method's robustness and consistency across a wide range of market conditions. Our results further demonstrate that the SWIFT method does not suffer the same drawback as the COS method when truncating the required integration range and adequately captures the mass of the underlying density function.

The rest of the paper is organised as follows. Section 2 introduces the proposed double exponential jump model with stochastic volatility and jump intensity, and presents a brief derivation of the resulting characteristic function. The SWIFT methodology to price power options is developed in Section 3, with our numerical experiments and sensitivity analysis conducted in Section 4. Finally, Section 5 concludes.

2. Model specification and characteristic function derivation

We let $(\Omega, \mathcal{F}_t, \mathbb{Q})$ be a complete probability space on which the Brownian motions W_t^s, W_t^v and W_t^λ, for $0 \le t \le T$, are defined. The filtration $\mathcal{F}_t$ is generated by the Brownian motions and the jump process, and $\mathbb{Q}$ is the risk-neutral probability under which the underlying asset price S_t, volatility process v_t and the jump intensity λ_t are governed by the following dynamics:

$$\begin{aligned} dS_t &= (r - \lambda_t\delta)S_t dt + \sqrt{v_t}S_t dW_t^s + S_t(e^Y - 1)dN_t, \\ dv_t &= (\theta_v - \alpha_v v_t)dt + \sigma_v\sqrt{v_t}dW_t^v, \\ d\lambda_t &= (\theta_\lambda - \alpha_\lambda\lambda_t)dt + \sigma_\lambda\sqrt{\lambda_t}dW_t^\lambda, \end{aligned} \tag{1}$$

where r represents the constant rate of interest. The long-term equilibrium mean levels for the stochastic volatility and jump intensity are all constant and denoted by θ_v and θ_λ, respectively. In addition, the mean-reverting rates, α_v and α_λ, and the volatility coefficients, σ_v and σ_λ, are all positive constants. N_t represents a Poisson process whereby the stochastic jump intensity, λ_t, has an average jump amplitude of $\delta = \mathbb{E}[e^Y - 1]$ under $\mathbb{Q}$, and Y is a random variable denoting the jump size. Furthermore, dW_t^s and dW_t^v are a pair of correlated Brownian motions with $dW_t^s dW_t^v = \rho dt$, while W_t^λ is a Brownian motion independent of both W_t^s and W_t^v. Finally, suppose that Y follows an asymmetric double exponential distribution $h(Y)$,

$$h(Y) = p[\eta_u e^{-\eta_u Y}\mathbf{1}_{(Y\ge 0)}] + q[\eta_d e^{\eta_d Y}\mathbf{1}_{(Y<0)}], \tag{2}$$

where p, q denotes the up-move and down-move probabilities, respectively, with $p + q = 1$. Moreover, $\eta_u > 1$, $\eta_d > 0$ are the mean positive and negative jumps, respectively. Hence, $\delta = \frac{p\eta_u}{\eta_u - 1} + \frac{q\eta_d}{\eta_d + 1} - 1$. We further assume that N_t and Y are independent of the Brownian motions defined above.

Given the stochastic price process in (1) above, we first solve for the moment generating function (MGF), $M(\Phi)$, of the log-asset price $X_T = \ln S_T$. Thereafter, we can easily obtain the complex-valued characteristic function $\phi(u)$ through the relationship $\phi(u) = M(iu)$. Under measure $\mathbb{Q}$, the MGF of X_T can be determined by:

$$M(\Phi) = \mathbb{E}[e^{\Phi X_T}|\mathcal{F}_t] = e^{-r(T-t)}\mathbb{E}[e^{r(T-t)}e^{\Phi X_T}|X_t = x, v_t = v, \lambda_t = \lambda]. \tag{3}$$

Hence, the MGF can also be defined as a contingent claim with payoff $e^{r(T-t)+\Phi X_T}$ at final time T. By applying the generalised form of the well-known Feynman-Kac formula (as provided in [4]) to (3) above (see [13,26,33]), we obtain the resulting partial integral-differential equation (PIDE) for $M(\Phi)$:

$$\begin{aligned} &-\tfrac{\partial M}{\partial t} + \left(r - \lambda\delta - \tfrac{v}{2}\right)\tfrac{\partial M}{\partial X} + \tfrac{1}{2}v\tfrac{\partial^2 M}{\partial X^2} + (\theta_v - \alpha_v v)\tfrac{\partial M}{\partial v} + \tfrac{1}{2}\sigma_v^2 v\tfrac{\partial^2 M}{\partial v^2} + \rho\sigma_v v\tfrac{\partial^2 M}{\partial X\partial v} + (\theta_\lambda - \alpha_\lambda\lambda)\tfrac{\partial M}{\partial\lambda} + \tfrac{1}{2}\sigma_\lambda^2\lambda\tfrac{\partial^2 M}{\partial\lambda^2} \\ &+\lambda\textstyle\int_{-\infty}^{\infty}[M(X+Y) - M(X)]f(Y)dY = 0. \end{aligned} \tag{4}$$

The above PIDE can be solved by postulating a solution of the form:

$$M(\Phi) = e^{\Phi r(T-t)+A(t,T)+B(t,T)+C(t,T)v+D(t,T)\lambda+\Phi \ln S_t}, \tag{5}$$

with zero boundary conditions for A, B, C and D. First, we consider the integral term in (4):

$$\begin{aligned}\lambda \int_{-\infty}^{\infty} [M(X+Y) - M(X)] f(Y) dY &= \lambda \int_{-\infty}^{\infty} \mathbb{E}[e^{\Phi X}]\mathbb{E}[e^{\Phi Y} - 1] f(Y) dY \\ &= \lambda M(\Phi)\delta_1,\end{aligned} \tag{6}$$

where $\delta_1 = \frac{p\eta_u}{\eta_u - \Phi} + \frac{q\eta_d}{\eta_d + \Phi} - 1$. It follows that by substituting Eqs. (5) and (6) into the PIDE (4) we obtain an equation that holds for all t, X, v and λ. Hence, we can reduce the problem to solving the following system of five, much simpler, ordinary differential equations:

$$\frac{\partial A(t,T)}{\partial t} + \frac{\partial B(t,T)}{\partial t} = \theta_v C(t,T) + \theta_\lambda D(t,T), \tag{7}$$

$$\frac{\partial C(t,T)}{\partial t} = \frac{1}{2}(\Phi^2 - \Phi) - (\alpha_v - \rho\sigma_v\Phi)C(t,T) + \frac{1}{2}\sigma_v^2 C^2(t,T), \tag{8}$$

$$\frac{\partial D(t,T)}{\partial t} = (\delta_1 - \delta\Phi) - \alpha_v D(t,T) + \frac{1}{2}\sigma_\lambda^2 D^2(t,T), \tag{9}$$

where

$$\frac{\partial A(t,T)}{\partial t} = \theta_v C(t,T), \tag{10}$$

$$\frac{\partial B(t,T)}{\partial t} = \theta_\lambda D(t,T). \tag{11}$$

From the above system of ODE's, we can first solve for the Riccati Eq. (9), whereby a general solution may be derived, followed by solving for (11). Thereafter, by analogy, we can solve for $C(t,T)$ and $A(t,T)$, respectively.

To solve for (9), we will require a particular solution from which to derive the general solution for the Riccati equation. Hence, we make the following substitution:

$$D(t,T) = \frac{-2w'(T-t)}{\sigma_\lambda^2 w}. \tag{12}$$

Substituting (12) into (9) above and simplifying we obtain the following ODE:

$$w''(T-t) + \alpha_\lambda w'(T-t) - \frac{1}{2}\sigma_\lambda^2(\delta\Phi - \delta_1)w(T-t) = 0, \tag{13}$$

which has a general solution of the form:

$$w(T-t) = U_1 e^{\frac{1}{2}\zeta_-(T-t)} + U_2 e^{\frac{1}{2}\zeta_+(T-t)}, \tag{14}$$

where $\zeta_\pm = \varphi \mp \alpha_\lambda$ and $\varphi = \sqrt{\alpha_\lambda^2 + 2\sigma_\lambda^2(\delta\Phi - \delta_1)}$. Both U_1 and U_2 are constants to be determined from the initial conditions $w(0) = U_1 + U_2$ and $w'(0) = 0$, since $D(T,T) = 0$. Solving for U_1 and U_2, we obtain the following solution:

$$U_1 = \frac{w(0)\zeta_+}{2\varphi} \quad \text{and} \quad U_2 = \frac{w(0)\zeta_-}{2\varphi}.$$

Substituting U_1 and U_2 into (14) above, we find the exact solution to (9):

$$D(t,T) = 2(\delta\Phi - \delta_1)\left\{\frac{1 - e^{\varphi(T-t)}}{\zeta_+ + \zeta_- e^{\varphi(T-t)}}\right\}. \tag{15}$$

Therefore, from (11), together with (12) and the solution in (15), we obtain:

$$B(t,T) = \theta_\lambda \int_t^T D(t,s)ds = -\frac{\theta_\lambda}{\sigma_\lambda^2}\left\{\zeta_+(T-t) + 2\ln\left[\frac{\zeta_- + \zeta_+ e^{-\varphi(T-t)}}{2\varphi}\right]\right\}.$$

Finally, solving for ODE's $A(t,T)$ and $C(t,T)$ by analogy, we obtain the following solutions:

$$A(t,T) = -\frac{\theta_v}{\sigma_v^2}\left\{\gamma_+(T-t) + 2\ln\left[\frac{\gamma_- + \gamma_+ e^{-\vartheta(T-t)}}{2\vartheta}\right]\right\},$$

$$C(t,T) = (\Phi - \Phi^2)\left\{\frac{1 - e^{\vartheta(T-t)}}{\gamma_+ + \gamma_- e^{\vartheta(T-t)}}\right\}.$$

where

$$\gamma_{\pm} = \pm(\rho\sigma_v\Phi - \alpha_v) + \vartheta,$$
$$\vartheta = \sqrt{(\rho\sigma_v\Phi - \alpha_v)^2 + \sigma_v^2(\Phi - \Phi^2)}.$$

From the above, we use $\phi(u) = M(iu)$ to obtain the required characteristic function of $\ln S_T$:

$$\phi(u) = e^{iur(T-t)+\bar{A}(t,T)+\bar{B}(t,T)+\bar{C}(t,T)v+\bar{D}(t,T)\lambda+iu\ln S_t}, \tag{16}$$

where

$$\bar{A}(t,T) = -\frac{\theta_v}{\sigma_v^2}\left[\gamma_+(T-t) + 2\ln\left(\frac{\xi_\gamma}{2\vartheta}\right)\right],$$
$$\bar{B}(t,T) = -\frac{\theta_\lambda}{\sigma_\lambda^2}\left[\zeta_+(T-t) + 2\ln\left(\frac{\xi_\zeta}{2\varphi}\right)\right],$$
$$\bar{C}(t,T) = (iu+u^2)\frac{1-e^{\vartheta(T-t)}}{\gamma_+ + \gamma_- e^{\vartheta(T-t)}},$$
$$\bar{D}(t,T) = 2(iuL_2 - L_1)\frac{1-e^{\varphi(T-t)}}{\zeta_+ + \zeta_- e^{\varphi(T-t)}},$$
$$\xi_\gamma = \gamma_- + \gamma_+ e^{-\vartheta(T-t)},$$
$$\xi_\zeta = \zeta_- + \zeta_+ e^{-\varphi(T-t)},$$
$$\gamma_{\pm} = \pm(iu\rho\sigma_v - \alpha_v) + \vartheta,$$
$$\zeta_{\pm} = \varphi \mp \alpha_\lambda,$$
$$\vartheta = \sqrt{(iu\rho\sigma_v - \alpha_v)^2 + \sigma_v^2(iu+u^2)},$$
$$\varphi = \sqrt{\alpha_\lambda^2 + 2\sigma_\lambda^2(iuL_2 - L_1)},$$
$$L_1 = \frac{p\eta_u}{\eta_u - iu} + \frac{q\eta_d}{\eta_d + iu} - 1,$$
$$L_2 = \frac{p\eta_u}{\eta_u - 1} + \frac{q\eta_d}{\eta_d + 1} - 1.$$

3. Shannon wavelet inverse Fourier technique (SWIFT)

The point of departure for the SWIFT method, as with other numerical integration techniques, is the discounted expectation of the option payoff at maturity under the risk-neutral measure $\mathbb{Q}$, i.e.

$$f(x,t) = e^{-r(T-t)}\mathbb{E}^{\mathbb{Q}}[f(y,T)|x] = e^{-r(T-t)}\int_{\mathbb{R}} f(y,T)g(y|x)dy, \tag{17}$$

where x and y are state variables at initial time t and maturity T, respectively. $g(y|x)$ is the conditional density under the risk-neutral measure, and r the risk-free rate of interest. If we define the log-asset state prices by $x := \ln S_t^\beta/K$ and $y := \ln S_T^\beta/K$, where K denotes the strike price and β the constant power term, then the final payoff function, f, can be expressed as[1]:

$$f(y,T) = \begin{cases} [K(e^y - 1)]^+ & \text{for a power call option,} \\ [K(1-e^y)]^+ & \text{for a power put option.} \end{cases} \tag{18}$$

While the COS method of [5] replaces the density function in (17) by its Fourier-cosine series expansion, the SWIFT method approximates density g by making use of a finite combination of Shannon scaling functions, at some chosen level (or scale) of approximation, m, then recovering the density coefficients of the approximation from its Fourier transform, i.e., the associated characteristic function. Hence, following the detailed derivations in [25], we have $g(x) \approx \mathcal{P}_m g(x) = \sum_{k\in\mathbb{Z}} c_{m,k}\psi_{m,k}(x)$, where the projection $\mathcal{P}_m g(.)$ converges to $g(.)$ as $m \to \infty$. $\psi_{m,k}(y) = 2^{m/2}\mathrm{sinc}(2^{\mathrm{m}}\mathrm{y} - \mathrm{k})$ is the Shannon scaling function, with $c_{m,k}(x) = \int_{\mathbb{R}} g(x)\psi_{m,k}(x)dx$ denoting the scaling or density coefficients. Given the above, our pricing Eq. (17) then follows with

$$f(x,t) \approx e^{-r(T-t)}\int_{\mathcal{D}_m} f(y,T)g_m(y|x)dy = e^{-r(T-t)}\sum_{k=k_1}^{k_2} c_{m,k}(x)\cdot V_{m,k}, \tag{19}$$

[1] The scaling of the log-asset prices to the strike price will allows us to price a basket of options in just a single calculation with a vector of strikes. We shall demonstrate this in the numerical experiments.

where $g(y|x) \approx g_m(y|x) = \sum_{k=k_1}^{k_2} c_{m,k}(x)\psi_{m,k}(y)$,[2] and $V_{m,k}$ are the payoff coefficients defined as

$$V_{m,k} := \int_{\mathcal{D}_m} f(y,T)\psi_{m,k}(y)dy. \tag{20}$$

The infinite integration can be truncated to a finite range $\mathcal{D}_m = [k_1/2^m, k_2/2^m]$ without significant loss of density mass for accurately chosen k_1 and k_2 values. One such truncation method is to utilise the cumulants, μ_n, as proposed in [5,24,25], and define the range

$$\left[x + \mu_1 - L\sqrt{\mu_2 + \sqrt{\mu_4}}; x + \mu_1 + L\sqrt{\mu_2 + \sqrt{\mu_4}}\right], \tag{21}$$

where, typically, $L = 10; 12$.[3] Note that the 4th cumulant, μ_4, is included to account for heavy tails and excess kurtosis exhibit in the density function of our proposed model in (1).

We emphasise at this point that the choice of parameter L is not immediately obvious, and the potential pricing errors as a result. This is particularly the case with call options, whereby the payoff function is generally unbounded and grows exponentially with respect to the log-asset price. Consequently, significant approximation errors may emerge when truncating the integration domain of the risk-neutral formula with large values of L. However, since put options are bounded by the strike price K, they do not suffer the same setback. Hence, we can utilise the put-call parity to obtain call option values once the put option prices are determined. This may provide slight improvements to the pricing accuracy [5]. In the sequel, we present a set of error analyses to demonstrate the convergence of call prices to increase in parameter L. This allows us to determine an appropriate choice of the parameter.

Given our payoff function f, as presented in (18), and the scaling function $\psi_{m,k}(y) = 2^{m/2}\mathrm{sinc}(2^{\mathrm{m}}\mathrm{y} - \mathrm{k})$, the payoff coefficients (20) may be expressed as:

$$\begin{aligned} V_{m,k} &= \begin{cases} \int_{\mathcal{D}_m}[K(e^y-1)]^+ \cdot 2^{m/2}\mathrm{sinc}(2^{\mathrm{m}}\mathrm{y}-\mathrm{k})\mathrm{dy} & \text{for a power call option,} \\ \int_{\mathcal{D}_m}[K(1-e^y)]^+ \cdot 2^{m/2}\mathrm{sinc}(2^{\mathrm{m}}\mathrm{y}-\mathrm{k})\mathrm{dy} & \text{for a power put option,} \end{cases} \\ &= \begin{cases} \int_{\mathcal{D}_m\cap[0,+\infty)} K(e^y-1)\cdot 2^{m/2}\mathrm{sinc}(2^{\mathrm{m}}\mathrm{y}-\mathrm{k})\mathrm{dy} & \text{for a power call option,} \\ \int_{(-\infty,0]\cap\mathcal{D}_m} K(1-e^y)\cdot 2^{m/2}\mathrm{sinc}(2^{\mathrm{m}}\mathrm{y}-\mathrm{k})\mathrm{dy} & \text{for a power put option.} \end{cases} \end{aligned} \tag{22}$$

By approximating the cardinal sinus function (see [8]), together with the cosine product-to-sum identity of [27], we have

$$V_{m,k} \approx V^*_{m,k} := \begin{cases} \frac{K2^{m/2}}{2^{J-1}} \sum_{j=1}^{2^{J-1}} \left[\Pi_{1,k}\left(\frac{\bar{k}_1}{2^m}, \frac{k_2}{2^m}\right) - \Pi_{2,k}\left(\frac{\bar{k}_1}{2^m}, \frac{k_2}{2^m}\right)\right] & \text{if } \mathrm{k}_2 > 0, \\ 0 & \text{if } \mathrm{k}_2 \le 0, \end{cases}$$

for a power call option, and

$$V_{m,k} \approx V^*_{m,k} := \begin{cases} \frac{-K2^{m/2}}{2^{J-1}} \sum_{j=1}^{2^{J-1}} \left[\Pi_{1,k}\left(\frac{k_1}{2^m}, \frac{\bar{k}_2}{2^m}\right) - \Pi_{2,k}\left(\frac{k_1}{2^m}, \frac{\bar{k}_2}{2^m}\right)\right] & \text{if } \mathrm{k}_1 > 0, \\ 0 & \text{if } \mathrm{k}_1 \ge 0, \end{cases}$$

for a power put. Where $\bar{k}_1 := \max(k_1, 0)$ and $\bar{k}_2 := \min(k_2, 0)$, and both functions $\Pi_{1,k}$ and $\Pi_{2,k}$ are given by Proposition 1 below.

Proposition 1. *The payoff coefficients, $\Pi_{1,k}$, of a function $\mathcal{H}(y) = e^y$ on $[c,d]$ is given by*

$$\Pi_{1,k}(c,d) := \int_c^d e^y \cos(\chi_j(2^m y - k))dy, \tag{23}$$

and the payoff coefficient, $\Pi_{2,k}$, of another function $\mathcal{H}(y) = 1$ on $[c,d]$ is given by

$$\Pi_{2,k}(c,d) := \int_c^d \cos(\chi_j(2^m y - k))dy, \tag{24}$$

where $\chi_j = \frac{2j-1}{2^J}\pi$, are both known analytically.

Proof. Firstly, as with the derivation of the density coefficients, the classical Vieta formula allows us to express the cardinal sinus function as an infinite product of cosine terms (see [8]). By truncating the infinite product to a domain with J factors only, the cosine product-to-sum identity allows us to approximate the cardinal sinus function as $\mathrm{sinc}(\mathrm{x}) \approx \mathrm{sinc}^*(\mathrm{x}) :=$

[2] The infinite summation in projection $\mathcal{P}_m g(x)$ can be accurately approximated by $g_m(x) := \sum_{k=k_1}^{k_2} c_{m,k}\psi_{m,k}(x)$ for appropriately chosen k_1 and k_2 values (see Lemma 1 of [25])

[3] justifications for the choice of L is further provided in Section 4.

$\frac{1}{2^{J-1}}\sum_{j=1}^{2^{J-1}}\cos\left(\frac{2j-1}{2^J}\pi x\right)$ (see [27]). Hence, by replacing the sinc functions in (22) with the approximation above, and defining $\chi_j = \frac{2j-1}{2^J}\pi$, we can obtain the following expressions:

$$\Pi_{1,k}(c,d) := \int_c^d e^y \cos(\chi_j(2^m y - k))dy,$$

and

$$\Pi_{2,k}(c,d) := \int_c^d \cos(\chi_j(2^m y - k))dy.$$

Thereafter, a straight forward calculation of the above integrals show that

$$\Pi_{1,k}(c,d) = \frac{\chi_j 2^m}{1+(\chi_j 2^m)^2}\left[e^d\sin\left(\chi_j(2^m d-k)\right) - e^c\sin\left(\chi_j(2^m c-k)\right) + \frac{1}{\chi_j 2^m}\left(e^d\cos\left(\chi_j(2^m d-k)\right) - e^c\cos\left(\chi_j(2^m c-k)\right)\right)\right],$$

and

$$\Pi_{2,k}(c,d) = \frac{1}{\chi_j 2^m}\left(\sin(\chi_j(2^m d-k)) - \sin(\chi_j(2^m c-k))\right).$$

□

Finally, since the cardinal sinus function can be approximated by a finite sum of cosine terms (see proof of Proposition 1 above), we can also approximate the scaling coefficients, $c_{m,k}$, by:

$$\begin{aligned} c_{m,k} \approx \tilde{c}_{m,k} &= \frac{2^{m/2}}{2^{J-1}}\sum_{j=1}^{2^{J-1}}\int_{\mathbb{R}} g(x)\cos\left(\frac{2j-1}{2^J}\pi\,(2^m x-k)\right)dx, \\ &= \frac{2^{m/2}}{2^{\bar{J}-1}}\mathrm{Re}\left[\sum_{j=0}^{2^{\bar{J}}-1}\phi^*\left(\frac{(2j+1)\pi 2^m}{2^{\bar{J}}}\right)e^{\frac{2\pi ikj}{2^{\bar{J}}}}e^{\frac{ik\pi}{2^{\bar{J}}}}\right], \end{aligned} \tag{25}$$

where $\int_{\mathbb{R}} g(x)\cos(ux)dx = \mathrm{Re}[\phi^*(u)]$, with $\mathrm{Re}[\cdot]$ denoted the real part of the argument, and $\phi^*(u)$ is the Fourier transform of the density function g associated with the scaled log-asset price $y = \ln S_T^\beta/K$, which may be obtained via (16) and Proposition 2 below.[4]

Noticeably, a change in the number of summation terms in (25) is possible if we assume $\phi^*(\frac{(2j+1)\pi 2^m}{2^{\bar{J}}}) = 0$ for $j = 2^{\bar{J}-1},\ldots,2^{\bar{J}}-1$. Hence, we can compute $\tilde{c}_{m,k}$ efficiently via the FFT algorithm. This will also require the selection of a constant $J = \bar{J}$ (instead of a varying J) for each value of k.[5]

Proposition 2. *Given the moment generating function, $M_X(u)$, of $X = \ln S_T$, then for constants $\beta, K > 0$, the moment generating function of $Y = \ln\left(\frac{S_T^\beta}{K}\right)$ is given by $M_Y(u) = e^{-u\ln K}M_X(\omega)$, where $\omega = u\beta$, and the resulting characteristic function is given by $\phi_Y(u) = e^{-iu\ln K}\phi_X(\omega)$.*

Proof. The MGF of Y is given by $M_Y(u) = \mathbb{E}\left(e^{u\ln(S_T^\beta/K)}\right) = e^{-u\ln K}M_X(\omega)$, since $e^{u\beta\ln S_T}$ is a monotonic function of $X = \ln S_T$. Hence, we have

$$M_Y(u) = e^{-u\ln K}M_X(\omega), \tag{26}$$

where $\omega = u\beta$. Finally, substituting iu for u in (26) above completes the proof. □

Following [25], the SWIFT power option pricing formula for a vector of strikes, $\mathbf{K}$, can be expressed as:

$$f(\mathbf{x},t) = e^{-r(T-t)}\frac{2^m\mathbf{K}}{2^{\bar{J}+\bar{J}-2}} \times \sum_{k=k_1}^{k_2}\mathrm{Re}\left[e^{\frac{ik\pi}{2^{\bar{J}}}}\sum_{j=0}^{2^{\bar{J}}-1}\phi^*\left(\frac{(2j+1)\pi 2^m}{2^{\bar{J}}};0\right)e^{-\frac{i(2j+1)\pi 2^m}{2^{\bar{J}}}\cdot\mathbf{x}}e^{\frac{2\pi ikj}{2^{\bar{J}}}}\right]\tilde{V}_{m,k}^*, \tag{27}$$

where

$$\tilde{V}_{m,k}^* := \begin{cases} \sum_{j=1}^{2^{J-1}}\left[\Pi_{1,k}\left(\frac{\bar{k}_1}{2^m},\frac{k_2}{2^m}\right) - \Pi_{2,k}\left(\frac{\bar{k}_1}{2^m},\frac{k_2}{2^m}\right)\right] & \text{if } k_2 > 0, \\ 0 & \text{if } k_2 \le 0, \end{cases}$$

[4] Note that for the SWIFT method we consider a probability density function g of the log-asset price y in $L^2(\mathbb{R})$ and its associated Fourier transform $\phi^*(u) = \int_{\mathbb{R}} e^{-iuy}g(y|x)dy$.

[5] We define the constant J by $\bar{J} := \lceil\log_2(\pi\Gamma_m)\rceil$, where $\Gamma_m := \max_{k_1<k<k_2}\Gamma_{m,k}$, with k_1 and k_2 fixed indices, and $\lceil x\rceil$ denoting the smallest integer greater than x. We define $\Gamma_{m,k} := \max(|2^m a-k|, |2^m a+k|)$ for some constant a such that $h(-a)+1-h(a) < \epsilon$ for $\epsilon > 0$ (see Theorem 1 of [25]).

Table 1
Number of terms used in SWIFT approximation based on size of interval determined by L with scale of approximation $m = 5$ and power $\beta = 1$.

L	10	12	14	18	26
k_1	−131	−156	−182	−233	−339
k_2	128	153	179	230	336

for a power call option, and

$$\tilde{V}^*_{m,k} := \begin{cases} \sum_{j=1}^{2^{J-1}} \left[\Pi_{1,k}\left(\frac{k_1}{2^m}, \frac{\bar{k}_2}{2^m}\right) - \Pi_{2,k}\left(\frac{k_1}{2^m}, \frac{\bar{k}_2}{2^m}\right) \right] & \text{if } k_1 < 0, \\ 0 & \text{if } k_1 \geq 0, \end{cases}$$

for a power put. This is possible since we have $\phi^*(u; x) = \phi^*(u; 0) \cdot e^{-iux}$.

Notably, the above simplification in (27) relaxes each $\tilde{V}^*_{m,k}$ from its dependence on the option strike prices, K, thus requiring only a single computation for each $k = k_1, \ldots, k_2$. Hence, we may price a basket of options across a range of strikes in a single numerical experiment through the expression above. It is also possible to further reduce the computational complexity of $V^*_{m,k}$ by choosing an appropriate constant $J = \tilde{J}$ value over all k, where $\tilde{J} := \lceil \log_2(\pi N) \rceil$ and $N := \max(|k_1|, |k_2|)$. Subsequently, the FFT algorithm may then be applied to speed up the computation (see Appendix B of [25]).

Finally, it is also worthwhile highlighting that one major advantage of utilising Shannon scaling functions is the convenience of determining the area under the approximated density function with minimal efforts once the coefficients $c_{m,k}$ are calculated. The approximated area may then be determined by (see [25]):

$$\tilde{H} = \frac{1}{2^{m/2}} \left(\frac{c_{m,k_1}}{2} + \sum_{k_1 < k < k_2} c_{m,k} + \frac{c_{m,k_2}}{2} \right), \tag{28}$$

where $\tilde{H} \approx 1$. Adequate determination of indices k_1 and k_2 with the cumulants, as discussed previously, are presented in our numerical experiments in Section 4. The closer the estimated area is to one, the more accurate our approximation of the target density function.

4. Numerical results

Our numerical experiments are carried out as follows. Firstly, we determine the appropriate choice for the scale of approximation, m, as well as the truncation range parameter, L, through three different methods by examining the convergence of the resulting approximation errors. Thereafter, we examine the pricing of power options with the SWIFT method, and compare the resulting prices to that of a Monte Carlo simulation as a benchmark to validate the method's pricing accuracy. To investigate the computational efficiency, we compare the CPU times required by the SWIFT method to that of the alternative COS and FFT methods. Finally, we demonstrate the model's robustness by exploring the sensitivity of the SWIFT option prices to changes in the parameters of our proposed stochastic model.

4.1. Integration range and scale of approximation

Following [13] for pricing comparisons, we utilise the initial parameters at time $t = 0$: $S_0 = 1, v_0 = 0.15, \lambda_0 = 3, r = 0.05, d = 0.05, \theta_v = 0.18, \alpha_v = 0.3, \sigma_v = 0.1, \theta_\lambda = 3, \alpha_\lambda = 5, \sigma_\lambda = 0.3, \rho = -0.25, \eta_u = 33.33, \eta_d = 7.69, T = 0.5$. We begin by identifying the truncation of the integration range required for both the SWIFT and COS methods in order to obtain the payoff coefficients. As mentioned in Section 3, this will require the cumulants of the scaled log-asset price $\ln(S_T^\beta/K)$, where the jth cumulant, μ_j, is calculated via the jth derivative of the MGF (3) evaluated at 0. Hence, following [5], the truncation domain to approximate the option prices is given by (21), where, typically, $L = 10; 12$. The choice of truncation parameter L is not immediately obvious, and further discussions and justifications for our choice are provided in the numerical experiments to follow. Readers can also refer to the seminal work of [5] for detailed discussions on the choice of cumulants to include in the truncation range, as well as the choice of the truncation parameter L. Table 1 presents the corresponding number of terms required in the SWIFT method approximation given a chosen value of L with $\beta = 1$. The equivalent number of terms required in the alternative COS method can also be determined.[6]

An adequate choice for the scale of approximation, m, upfront is important given that it cannot be re-adjusted at a later stage without recalculating all approximation terms. Hence, along the lines of [24], we utilise the Fourier transform, $\phi^*(u)$, of the density function to determine the appropriate choice of wavelet scale, m, in analytical form. This is possible since our stochastic process of interest (1) satisfies the following condition:

$$\left|\phi^*(u)\right| = \left|e^{\Theta(u)(T-t)}\right| \leq \mathcal{C} e^{-\tilde{d}(T-t)|u|^\kappa}, \tag{29}$$

[6] For example, a choice of $L = 14$ will required $N \approx 360$

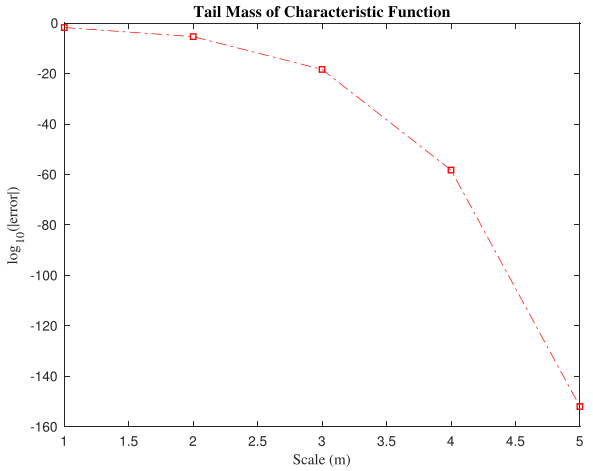

Fig. 1. Tail Mass of Characteristic Function Not Recovered.

with $\kappa = 2$ and constants $\mathcal{C}, \tilde{d} > 0$.[7] $\Theta(u)$ the characteristic exponent of (1). From (29), it can be shown through integration that the mass of the tails of the characteristic function, $\mathcal{A}(2^m\pi)$, is bounded by

$$\mathcal{A}(2^m\pi) \leq \frac{\mathcal{C}}{\pi\kappa(\tilde{d}(T-t))^{1/\kappa}}\Gamma\left(\frac{1}{\kappa}, \tilde{d}(T-t)(2^m\pi)^\kappa\right) =: \epsilon_m, \tag{30}$$

where Γ represents the incomplete gamma function, and

$$\epsilon_m \sim \frac{\mathcal{C}(2^m\pi)^{1-\kappa}}{\pi\kappa\tilde{d}(T-t)} e^{-\tilde{d}(T-t)(2^m\pi)^\kappa}, \tag{31}$$

for large values of $2^m\pi$ (see [24]). Note that (31) holds uniformly for all u. From (31), it can also be observed that ϵ_m converges exponentially with respect to m. However, since parameters $\mathcal{C}$ and $\tilde{d}$ are not available in most cases, we overcome the drawback by allowing the substitution of $\mathcal{C}e^{-\tilde{d}(T-t)|u|^\kappa} \sim |\phi^*(\pm 2^m\pi)|$ into (31). Hence, ϵ_m can we approximated by,

$$\epsilon_m \sim \frac{(2^m\pi)^{1-\kappa}}{2\pi\kappa(T-t)}\left(\left|\phi^*(-2^m\pi)\right| + \left|\phi^*(2^m\pi)\right|\right). \tag{32}$$

Using (32) above, we may efficiently compute the approximation error for a particular choice of wavelet scale, m, without a significant amount of CPU time. Hence, we can carry out a straight forward iterative procedure, through choosing $m = 0, 1, 2, \ldots$ until ϵ_m is less than a tolerance level, TOL, determined a priori.

From Fig. 1 we observe that, by setting a tolerance level of $TOL = 10^{-99}$, say, then the iterative procedure with (32) through choices of $m = 0, 1, 2, \ldots$ would identify $m = 5$ as an adequate wavelet scale of approximation. Notably, a lower choice of tolerance level by the user may deem $m = 3$, say, as an appropriate choice for the scale of approximation. It is also worthwhile noting that the CPU time required almost doubles, without significant recovery of the density mass lost, when increasing the scale of approximation from $m = 5$ to $m = 6$.

In addition to the above, we demonstrate that the rate of convergence of the SWIFT option prices to increasing wavelet scale of approximation, m, is exponential for both the vanilla European calls and puts (see Fig. 2). Moreover, similar findings across a range of power, β, are illustrated in Fig. 3. In both cases, we define the relative error as the percentage of absolute price differences for each option when referenced to a benchmark price with $m = 8$.

Recall that a major advantage of utilising Shannon scaling function is the ability to determine the area under the approximated density function with minimal efforts once the coefficients $c_{m,k}$ are calculated (see Section 3). The approximated area may then be determined by (28). Figure 4 presents the error convergence in the density approximation with the SWIFT method. Evidently, the error convergence in the density approximation is also exponential, with negligible differences for $m > 5$.

Finally, to further complement the findings of [5,25], justifications for our choice of the truncation parameter, L, when identifying an appropriate truncation range, may be provided by conducting a numerical experiment to evaluate the price convergence in the parameter L. We demonstrate this in Fig. 5, which shows robustness for the choice of $L = 10 \sim 12$ across different scales of approximation, m.

[7] Note that κ may take on different values depending on the expression of $\phi^*(u)$.

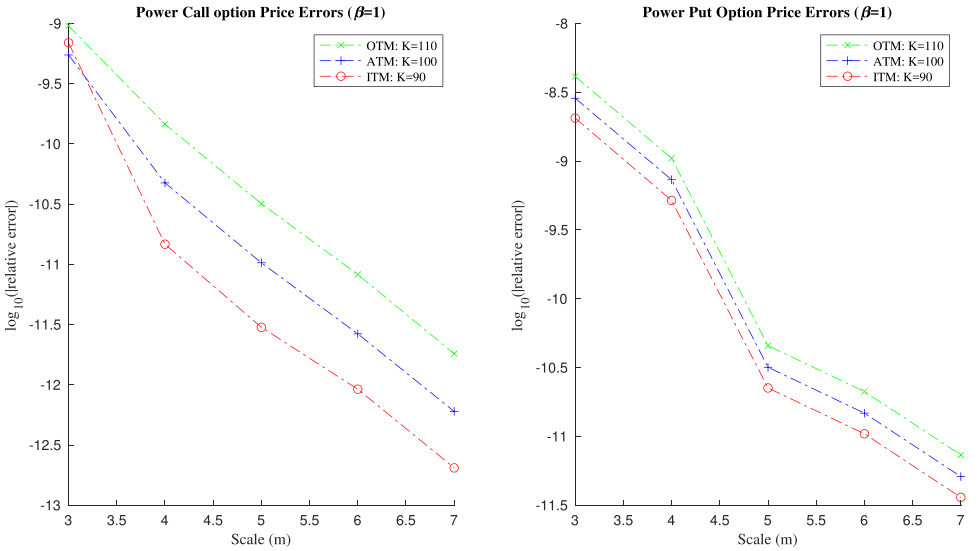

Fig. 2. SWIFT option price error convergence on increasing scale of approximation (m).

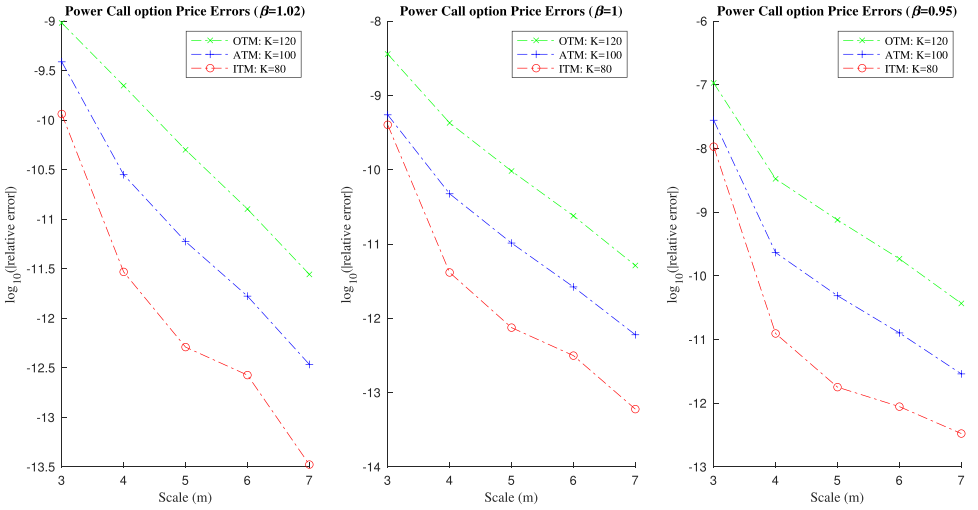

Fig. 3. SWIFT power option price convergence with increasing scale of approximation (m).

4.2. Power option pricing

Utilising the model parameters introduced at the beginning of Section 4.1 above, we price power call options with the SWIFT method across different powers, β, and compare our results to the corresponding option prices from the FFT and COS methods. Figure 6 presents the prices of a basket of power call options across a range of strikes. Additionally, we reveal the option price differences between the SWIFT and that of the COS method. When benchmarked to the COS prices, we observe that the SWIFT method is accurate and robust with minimal pricing errors across different moneyness of the option, as well as the various powers for the option payoff. In terms of efficiency, the COS method consumes 3.1 milliseconds on average, while the SWIFT method takes a mere 0.63 milliseconds to obtain the option prices.[8] All numerical experiments were conducted on a 3.9GHz quad-core Intel Core i7 machine with 16GB RAM.

Our results are further benchmarked against the option prices from a set of Monte Carlo simulations with 10^6 sample paths to confirm the accuracy in the pricing. It is also worthwhile noting that for sophisticated stock price processes, such as the proposed (1) above, situations may arise whereby consistent prices between the various Fourier-based methods are realised even though errors may exist in the computation of the characteristic function. Hence, including a comparison to methods that are independent of the characteristic function may provide further evidence of pricing accuracy.

[8] Note: computing times were averaged over 10^4 iterations.

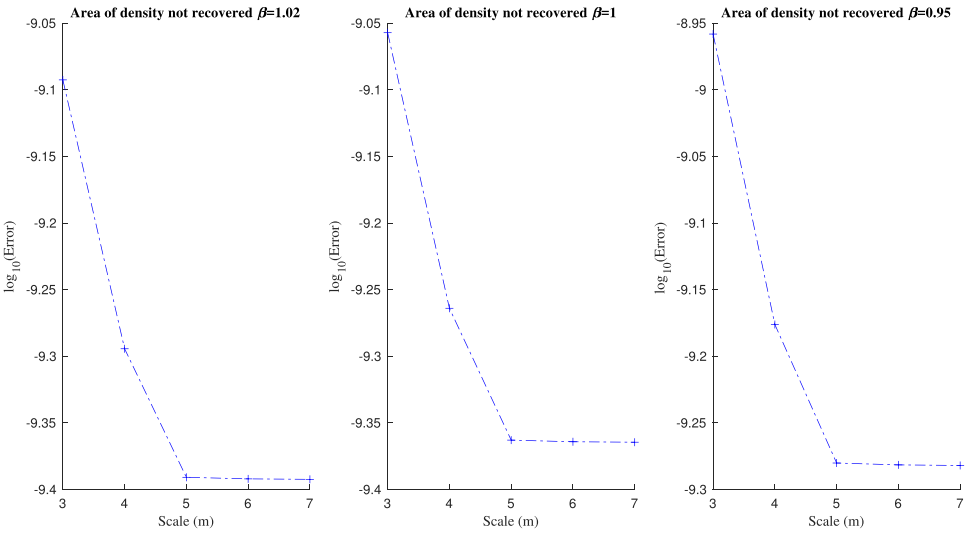

Fig. 4. Convergence of density mass lost from approximation under the SWIFT method.

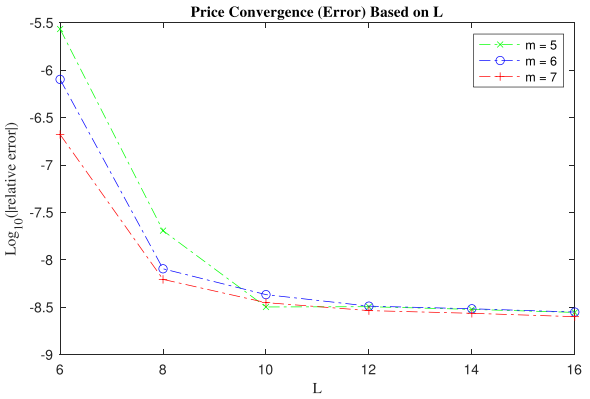

Fig. 5. SWIFT option price error convergence on increasing truncation range parameter L.

In order to carry out the Monte Carlo simulations, we first discretise the asset price dynamics (1) as follows:

$$\begin{aligned}
\ln S_{t+\Delta t} &= \ln S_t + (r - d - \lambda_t \delta)\Delta t + \sqrt{v_t}\mathcal{E}_1\sqrt{\Delta t} + (e^Y - 1)\ln S_t (N_{t+\Delta t} - N_t),\\
v_{t+\Delta t} &= v_t + (\theta_v - \alpha_v v_t)\Delta t + \sigma_v\sqrt{v_t}(\rho\mathcal{E}_1 + \sqrt{1-\rho^2}\mathcal{E}_2)\sqrt{\Delta t},\\
\lambda_{t+\Delta t} &= \lambda_t + (\theta_\lambda - \alpha_\lambda\lambda_t)\Delta t + \sigma_\lambda\sqrt{\lambda_t}\mathcal{E}_3\sqrt{\Delta t},
\end{aligned}$$

where t is the current time step, and Δt represents the length of time per simulated step. The terms $\mathcal{E}_1, \mathcal{E}_2$, and $\mathcal{E}_3$ are independent random variables sampled from a standard normal distribution. Option values can be obtained once the various sample paths for the final asset price at maturity T have been simulated with the discretisation above. The valuation then follows with the usual discounted expectation of the final option payoff. Resulting price comparisons, across different power values, β, are shown inTables 2–4.

Our numerical experiments demonstrate that the SWIFT method is highly accurate in the pricing of power options under our proposed asset price framework. This is clearly illustrated from the marginal price differences between the SWIFT method and the Monte Carlo simulations across a range of strikes (see Tables 2–4). In addition, the consistency of such marginal price differences are observed across different powers, β, which further advocates the method's accuracy and robustness. Moreover, the minimal price differences when compared to other state-of-the-art methods, such as the FFT and COS, further displays the high accuracy of the SWIFT method.

Further to the above-mentioned, the error analysis from our numerical examples in Section 4.1 demonstrate the SWIFT method's ability to price accurately in our proposed framework even without tight restrictions, such as the need for a relatively large integration range (through truncation range parameter, L), or a high scale of approximation, m. This is evident from the fast convergence of the resulting errors across the different scenarios of relaxing the above restrictions, as depicted in Figs. 1–5.

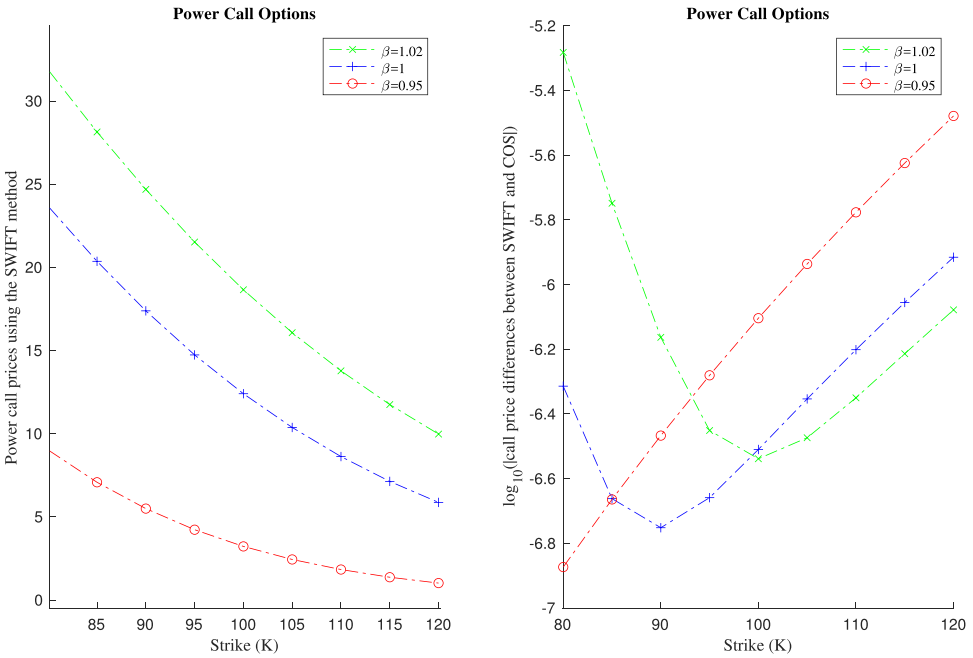

Fig. 6. Power call option prices under the SWIFT method, and the resulting price differences between SWIFT and COS methods.

Table 2
Power call price differences and relative error between SWIFT vs FFT / COS / M.C. methods for $\beta = 1$.

Power call option prices							
Strike	SWIFT	FFT	% diff.	COS	% diff.	M.C.	% diff.
85	20.3618	20.3618	1.0781e-06	20.3618	1.1061-06	20.3809	0.0938
90	17.3847	17.3847	1,0843e-06	17.3847	1.0844e-06	17.3737	0.0630
95	14.7344	14.7344	1.6057e-06	14.7344	1.6058e-06	14.7571	0.1541
100	12.4025	12.4025	3.8129-06	12.4025	3.8130e-06	12.4089	0.0511
105	10.3731	10.3730	4.6265-06	10.3730	4.6266e-06	10.3555	0.1689
110	8.62449	8.6245	7.9017-06	8.6245	7.9018e-06	8.6310	0.0753
115	7.13180	7.1318	1.3375-05	7.1318	1.3375e-05	7.1601	0.3967

Table 3
Power call price differences and relative error between SWIFT vs COS / M.C. methods for $\beta = 0.95$.

Power call option prices					
Strike	SWIFT	COS	% difference	M.C.	% difference
85	7.0773	7.0773	3.3158e-06	7.0849	0.1063
90	5.4957	5.4957	6.7267e-06	5.4874	0.1509
95	4.2264	4.2264	1.3436e-05	4.2376	0.2634
100	3.2224	3.2224	2.6464e-05	3.2233	0.0279
105	2.4382	2.4382	5.1459e-05	2.4255	0.5205
110	1.8324	1.8324	9.8886e-05	1.8325	0.0016
115	1.3691	1.3691	1.8795e-04	1.3739	0.3476

4.3. Price sensitivity to changes in model parameters

Finally, we evaluate the sensitivity of SWIFT power option prices to changes in the underlying model parameters. Fig. 7(a) demonstrates the changes in option prices to increases in the mean-reversion rate of jump intensity. By setting the long term intensity to 3, option prices with initial intensity less than the long term intensity increases with increasing rate of reversion, and the opposite is true for higher initial intensity values. This is reasonable as increases (decreases) in the number of jumps increases (decreases) the variability in the underlying asset price, and increases (decreases) the resulting call value. Similar evidence is found in Fig. 7(b) when evaluating a long term volatility of 0.15. Faster rates of reversion increases the value of

Table 4
Power call price differences and relative error between SWIFT vs COS / M.C. methods for $\beta = 1.02$.

Power call option prices					
Strike	SWIFT	COS	% difference	M.C.	% difference
85	28.1385	28.1385	6.3596e-06	28.1731	0.1232
90	24.6862	24.6862	2.8151e-06	24.7104	0.0981
95	21.5221	21.5221	1.7005e-06	21.5539	0.1475
100	18.6517	18.6517	1.6471e-06	18.6392	0.0670
105	16.0729	16.0729	2.2506e-06	16.1128	0.2488
110	13.7771	13.7771	3.5048e-06	13.7782	0.0080
115	11.7507	11.7507	5.6329e-06	11.7389	0.1001

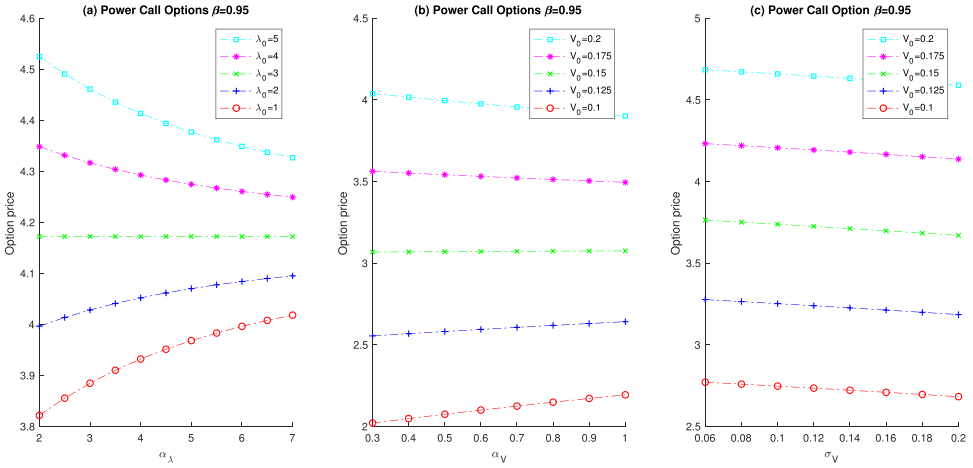

Fig. 7. Power call option price sensitivity to changes in underlying model parameters with β=0.95.

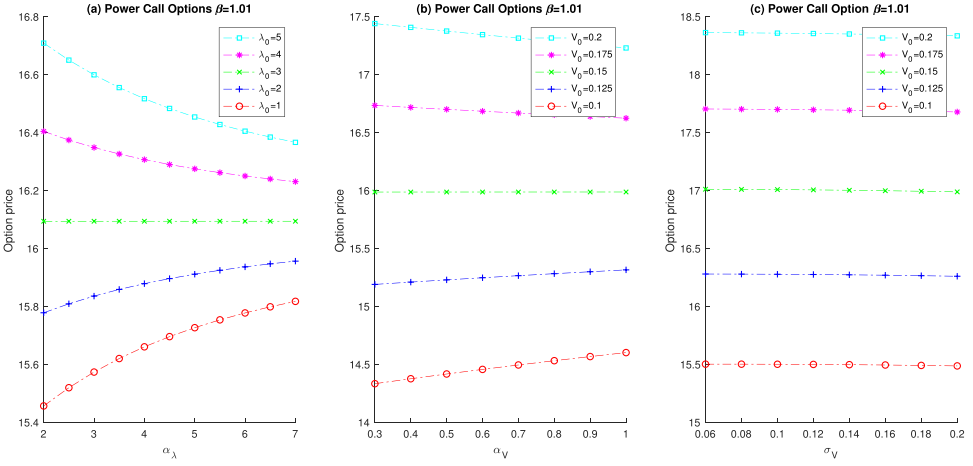

Fig. 8. Power call option price sensitivity to changes in underlying model parameters with β=1.01.

calls with a lower initial volatility, and the opposite is true for higher initial volatility values. Lastly, Fig. 7(c) demonstrate the changes in power call option prices to changes in the volatility of volatility.

In addition to the above, we analyse the consistency in the model sensitivities for changes in power β, and present our findings in Fig. 8. Our results demonstrate similar sensitivity patterns to those observed in the case where $\beta = 0.95$, providing further evidence in support of model robustness with the SWIFT method across a wide range of market conditions under our proposed framework.

5. Conclusion

In this paper, we proposed a highly efficient pricing method for power options using Shannon wavelets. In particular we advocate the use of a double exponential jump model with stochastic volatility and jump intensity for the underlying asset price dynamics. The characteristic function required for the SWIFT method pricing is derived through applying the generalised Feynman-Kac formula, and solving the resulting PIDE with a straight forward calculation. Results from our numerical experiments suggest that the SWIFT method is both accurate and robust, and more efficient than the novel Fourier-cosine method. Finally, we performed a set of sensitivity analyses to demonstrate the stability of the SWIFT method to changes in the underlying model parameters. The findings show that the resulting power option price responds reasonably to changes in the underlying model parameters, hence suggesting model robustness across different market conditions and advocating the use of our proposed stochastic model. Further studies may include the investigation of the SWIFT method in pricing early exercise exotics with our proposed asset price framework.

Acknowledgement

The financial assistance of the National Research Foundation (NRF) of South Africa and the University of Cape Town (UCT) towards this research is hereby acknowledged by C.-S. Huang. This work is based on the research supported in part by the NRF of South Africa for the grant, Unique Grant No. 94128. Any opinion, finding and conclusion or recommendation expressed in this material is that of the authors and both the NRF and UCT does not accept any liability in this regard.

References

[1] P. Carr, D. Madan, Option valuation using the fast Fourier transform, J. Comput. Finance 2 (4) (1999) 61–73.
[2] C. Chang, C.-D. Fuh, S.-K. Lin, A tale of two regimes: theory and empirical evidence for a Markov-modulated jump diffusion model of equity returns and derivative pricing implications, J. Bank. Finance 37 (8) (2013) 3204–3217.
[3] G. Colldeforns-Papiol, L. Ortiz-Gracia, C.W. Oosterlee, Two-dimensional Shannon wavelet inverse fourier technique for pricing european options, Appl. Numer. Math. 117 (2017) 115–138.
[4] D. Duffie, J. Pan, K. Singleton, Transform analysis and asset pricing for affine jump-diffusions, Econometrica 68 (6) (2000) 1343–1376.
[5] F. Fang, C.W. Oosterlee, A novel pricing method for european options based on fourier-cosine series expansions, SIAM J. Sci. Comput. 31 (2) (2008) 826–848.
[6] F. Fang, C.W. Oosterlee, Pricing early-exercise and discrete barrier options by fourier-cosine series expansions, Numer. Math. 114 (1) (2009) 27–62.
[7] F. Fang, C.W. Oosterlee, A fourier-based valuation method for bermudan and barrier options under Heston's model, SIAM J. Financ. Math. 2 (1) (2011) 439–463.
[8] W.B. Gearhart, H. Schultz, The function sin (x) x, Coll. Math. J. 2 (2) (1990) 90–99.
[9] S.L. Heston, A closed-form solution for options with stochastic volatility with applications to bond and currency options, Rev. Financ. Stud. 6 (2) (1993) 327–343.
[10] R.C. Heynen, H.M. Kat, Pricing and hedging power options, Financ. Eng. Jpn. Mark. 3 (3) (1996) 253–261.
[11] C.-S. Huang, J.G. O'Hara, S. Mataramvura, Efficient pricing of discrete arithmetic asian options under mean reversion and jumps based on Fourier-cosine expansions, J. Comput. Appl. Math. 311 (2017) 230–238.
[12] J. Huang, W. Zhu, X. Ruan, Fast Fourier transform based power option pricing with stochastic interest rate, volatility, and jump intensity, J. Appl. Math. 2013 (2013).
[13] J. Huang, W. Zhu, X. Ruan, Option pricing using the fast Fourier transform under the double exponential jump model with stochastic volatility and stochastic intensity, J. Comput. Appl. Math. 263 (2014) 152–159.
[14] S. Huang, X. Guo, A Fourier-cosine method for pricing discretely monitored barrier options under stochastic volatility and double exponential jump, Math. Probl. Eng. 2020 (2020).
[15] J. Hull, A. White, The pricing of options on assets with stochastic volatilities, J. Finance 42 (2) (1987) 281–300.
[16] A. Hurn, K. Lindsay, A. McClelland, On the efficacy of Fourier series approximations for pricing european options, Appl. Math. 5 (17) (2014) 2786–2807.
[17] S.N. Ibrahim, J.G. O'Hara, N. Constantinou, Pricing power options under the Heston dynamics using the FFT, New Trends Math. Sci. 1 (1) (2013) 1–9.
[18] S.N.I. Ibrahim, J.G. O'Hara, N. Constantinou, Risk-neutral valuation of power barrier options, Appl. Math. Lett. 26 (6) (2013) 595–600.
[19] J.L. Kirkby, Efficient option pricing by frame duality with the fast Fourier transform, SIAM J. Financ. Math. 6 (1) (2015) 713–747.
[20] S.G. Kou, A jump-diffusion model for option pricing, Manage. Sci. 48 (8) (2002) 1086–1101.
[21] S.G. Kou, H. Wang, Option pricing under a double exponential jump diffusion model, Manage. Sci. 50 (9) (2004) 1178–1192.
[22] A. Leitao, L. Ortiz-Gracia, E.I. Wagner, Swift valuation of discretely monitored arithmetic asian options, J. Comput. Sci. 28 (2018) 120–139.
[23] S. Macovschi, F. Quittard-Pinon, On the pricing of power and other polynomial options, J. Derivatives 13 (4) (2006) 61–71.
[24] S.C. Maree, L. Ortiz-Gracia, C.W. Oosterlee, Pricing early-exercise and discrete barrier options by Shannon wavelet expansions, Numer. Math. 136 (4) (2017) 1035–1070.
[25] L. Ortiz-Gracia, C.W. Oosterlee, A highly efficient Shannon wavelet inverse Fourier technique for pricing european options, SIAM J. Sci. Comput. 38 (1) (2016) B118–B143.
[26] E. Pillay, J. O'Hara, FFT based option pricing under a mean reverting process with stochastic volatility and jumps, J. Comput. Appl. Math. 235 (12) (2011) 3378–3384.
[27] B. Quine, S. Abrarov, Application of the spectrally integrated Voigt function to line-by-line radiative transfer modelling, J. Quant. Spectrosc. Radiat. Transf. 127 (2013) 37–48.
[28] M.J. Ruijter, C.W. Oosterlee, A Fourier cosine method for an efficient computation of solutions to BSDEs, SIAM J. Sci. Comput. 37 (2) (2015) A859–A889.
[29] P. Santa-Clara, S. Yan, Crashes, volatility, and the equity premium: lessons from s&p 500 options, Rev. Econ. Stat. 92 (2) (2010) 435–451.
[30] R. Tompkins, Power options: hedging nonlinear risks, J. Risk 2 (2000) 29–46.
[31] J. Topper, Finite element modeling of exotic options, in: Operations Research Proceedings 1999, Springer, 2000, pp. 336–341.
[32] G. Tour, N. Thakoor, A. Khaliq, D. Tangman, COS method for option pricing under a regime-switching model with time-changed Lévy processes, Quant. Finance 18 (4) (2018) 673–692.
[33] H.Y. Wong, Y.W. Lo, Option pricing with mean reversion and stochastic volatility, Eur. J. Oper. Res. 197 (1) (2009) 179–187.
[34] U. Wystup, Structured products, FX Opt. Struct. Prod. (2006) 139–209.
[35] B. Zhang, C.W. Oosterlee, Efficient pricing of european-style asian options under exponential Lévy processes based on Fourier cosine expansions, SIAM J. Financ. Math. 4 (1) (2013) 399–426.
[36] S. Zhang, J. Geng, Fourier-cosine method for pricing forward starting options with stochastic volatility and jumps, Commun. Stat.-Theory Methods 46 (20) (2017) 9995–10004.